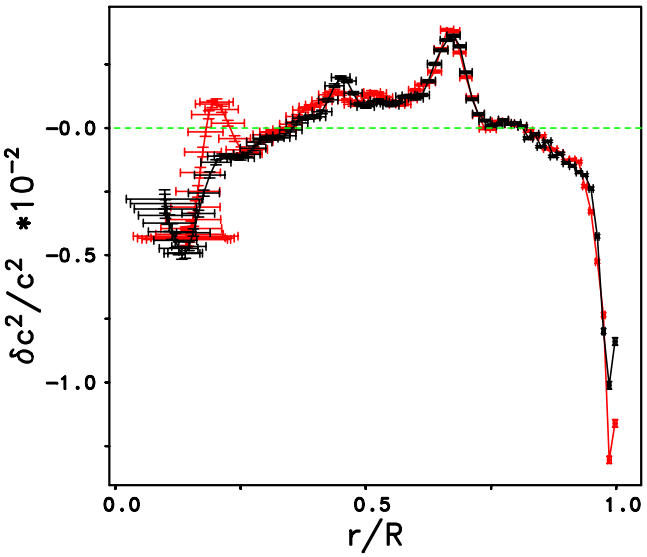

Figure 27. In red are shown the relative squared sound-speed deviations from the Standard Solar Model S of Christensen-Dalsgaard et al. (1996) in the sense "Sun minus Model" as a function of fractional radius that we obtained by a structural inversion of the 6,677 frequencies and their uncertainties that were computed using the MPTS method on the power spectra obtained from the $\mathcal{R}$2010_66 observing run. The horizontal bars represent the width ("spread") of the localized averaging kernels, providing a characteristic of the spatial resolution, while the vertical bars are the $1\,\sigma$ formal error estimates. For comparison is overlayed in black the inversion profile that we obtained by a structural inversion of the 6,685 WMLTP frequencies and their uncertainties. Both sets of frequencies covered the same frequency range from 965 to 4600 μHz. The dashed green line is for a deviation of zero.

deeper interior but also close to the surface in an upcoming study. Such study requires, however, observing runs lasting longer than 66 days and which are, furthermore, from different epochs.

In spite of the differences between the MPTS and WMLTP profile, our conclusions drawn in Paper I remain still valid. First, there is a substantial deviation from Model S near the surface which coincides with the sub-surface rotational shear layer. Second, the stratification of the convection zone and heat transport properties may be significantly different from the predictions of the mixing length theory (see, for example, Vitense (1953)). Third, the sound speed in both the outer half of the convection zone and in the sub-surface shear layer is systematically lower than the sound speed in the standard solar model.

7. HELIOSEISMIC INVERSION FOR SOLAR ROTATION

If the Sun were spherically symmetric, its oscillation frequencies would depend on radial order n and degree l but not on azimuthal order m. Hence, for each pair (n, l) there is a $(2l+1)$-fold degeneracy. However, the rotation of the Sun breaks the spherical symmetry and lifts the degeneracy. Moreover, advection causes modes that propagate in the direction of solar rotation to have higher frequencies than modes with the same resonant properties propagating in the opposite direction. The magnitude of this "rotational frequency splitting" is determined by the rotation rate in the region where a given mode is trapped. Since each mode of solar oscillation is trapped in a different region, it is possible to infer the rotation rate in the solar interior as functions of radial distance and latitude by studying the frequency-splitting coefficients (cf. Equation (25)) for all these modes. Here we have used a

standard two-dimensional regularized least-squares (RLS) technique, which seeks to balance fitting the data with the smoothness of the solution (see, for example, Schou et al. 1992, 1994). To get the internal angular velocity distribution shown in the left-hand panel of Figure 28, we inverted the 6,655 frequency splittings and their uncertainties that were computed by employing the MPTS method on the power spectra obtained from the $\mathcal{R}$2010_66 observing run. The trade-off parameters, which serve to suppress rapid variations in an RLS inversion, were assigned values of 10^{-4} and 10^{-2} for the radial and latitudinal regularization terms, respectively (see Equation (28) of Larson & Schou 2015). We note that the $\mathcal{R}$2010_66 observing run extended over more than two consecutive solar rotations, so that short-lived dynamical structures associated with individual active regions would have been averaged out of the inversion. For comparison we show in the right-hand panel of Figure 28 the internal angular velocity distribution obtained from the same set of data, except that only modes with degrees $l \leq 300$ were taken into account in the inversion procedure. The most-notable differences between the two inversions appear between fractional radii of 0.95 and 1.0 at the middle-latitudes. It seems that the high-degree inversion (left panel) has smoother near-surface angular velocity gradients at latitudes between 45 and 60 degrees, as can also been seen by comparing the radial profiles for these latitudes in the two panels of Figure 30.

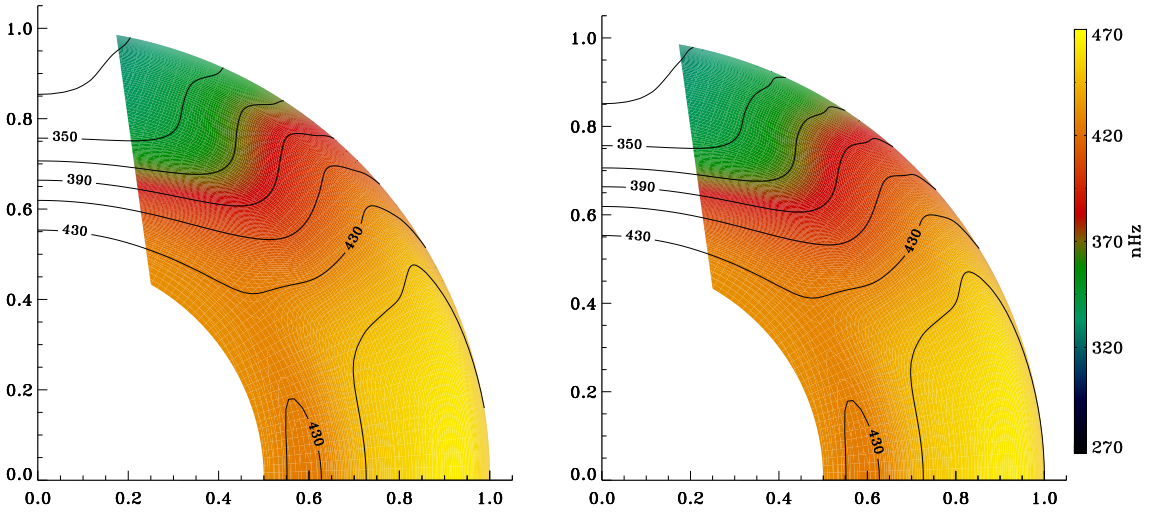

Figure 28. (Left) Inferred rotation rate in a quadrant of the Sun, obtained by means of inversion of the set of MPTS frequency-splitting coefficients derived from the $\mathcal{R}$2010_66 observing run using modes with degrees up to $l = 1000$. The equator is at the horizontal axis, and the pole is at the vertical axis. Both axes are labelled by fractional radius. From regions where the estimates of the rotation are deemed unreliable we have erased color while retaining the contours for ease of labeling. The contour spacing is 20 nHz; the highest contour line is at 450 nHz. (Right) Same as left panel, except that from the table of the MPTS frequency-splitting coefficients only modes with degrees up to $l = 300$ were taken into account in the inversion procedure. The color key indicates the rotation rate in nHz.

To illustrate the improvement in the inversions from adding the higher degree modes, Figure 29 shows cuts in radius of selected averaging kernels. An averaging kernel determines how the inversion actually averages the rotation rate over the interior of the Sun. For the targets near the surface (bottom row) the kernels are substantially narrower and have a weaker tail toward the center. At the same time, the noise is decreased. For the deeper targets, the kernels have reduced contributions

near the surface and thus less contamination, while the errors are roughly the same. In other words, the inversion is substantially improved if higher degree modes are included.

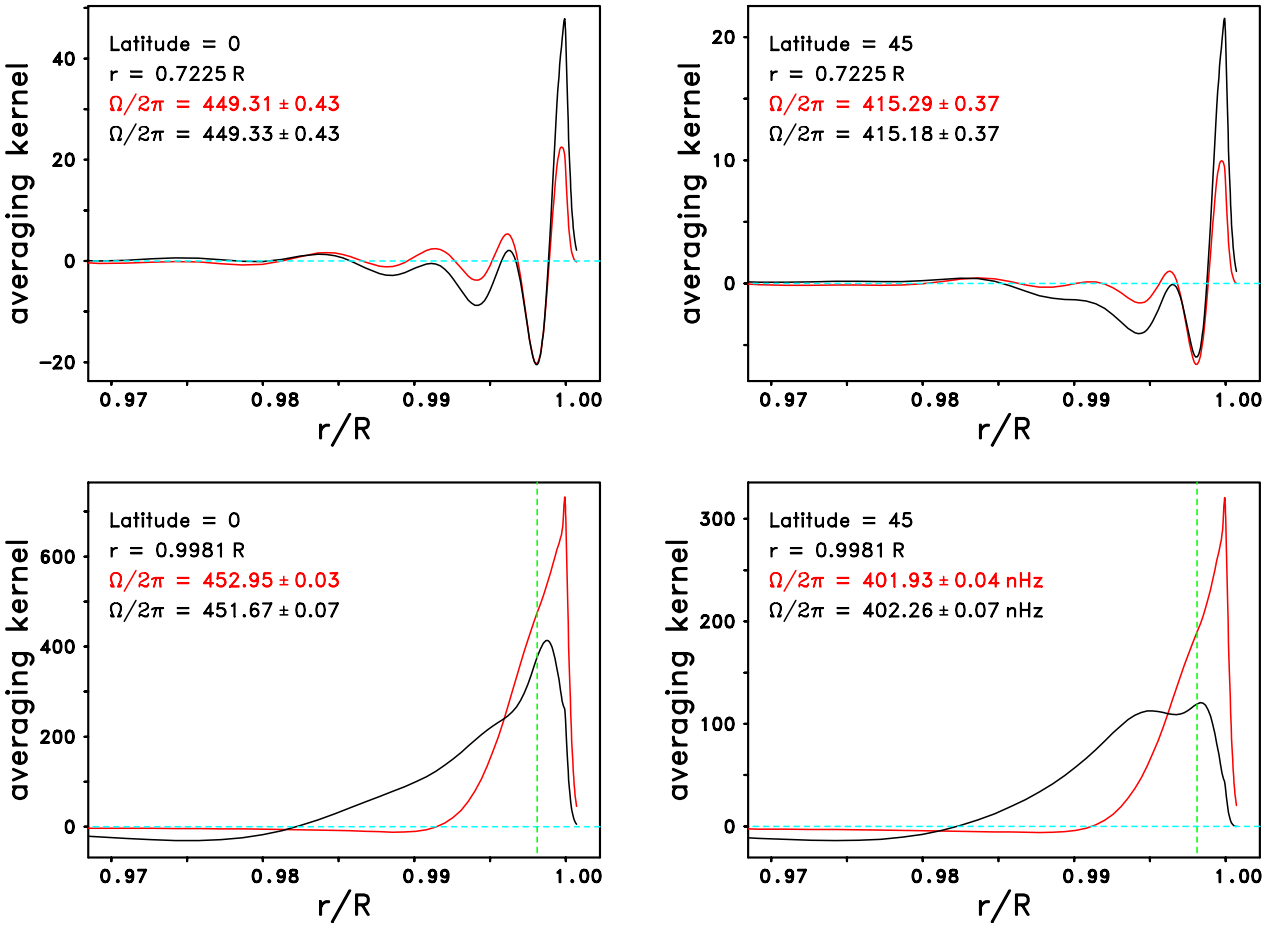

Figure 29. Averaging kernels as function of fractional radius, r/R, for two latitudes and two different target radii, r, where, R is the radius of the Sun. The kernels shown in red were inferred from the set of MPTS frequency-splitting coefficients obtained from the $\mathcal{R}$2010_66 observing run using modes with degrees up to $l = 1000$, while those shown in black include only modes with degrees up to $l = 300$. In each panel the rotation rate, $\Omega/2\pi$, and its associated uncertainty at approximately the target radius and latitude is shown in red when inferred from the mode set up to $l = 1000$, while it is shown in black when inferred from the mode set up to $l = 300$. The vertical dashed green lines in the bottom row represent the locations of the target radii of the averaging kernels. In the top row those lines are outside the plotting range. We note, however, that for the two cases shown in the top row the kernels are essentially identical near the target radius. The horizontal dashed turquoise lines represent the zero-line. The different scalings of the vertical axes in the panels are to be noted.

In order to better highlight both the similarities and the differences between the two rotational inversions shown in Figure 28, we show in Figure 30 the radial profiles of the rotation rate along the latitudes of 0 (black), 15 (red), 30 (green), 45 (blue), 60 (yellow), and 75 (magenta) degrees. In the left-hand panel of Figure 30 the results from the high-degree inversion are shown, while we show those from the intermediate-degree inversion in the right-hand panel. The common features of both panels in Figure 30 include 1) the Sub-surface Shear Layer (SSL, "leptocline"), 2) the shear

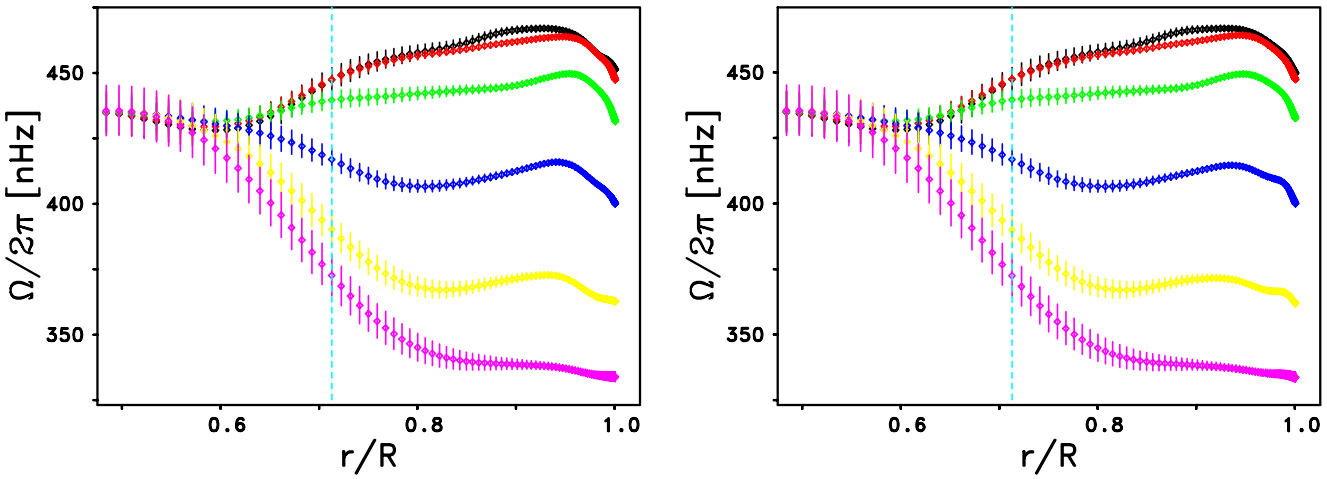

Figure 30. (Left) Rotation rate, measured in nHz, at latitudes of 0 (black), 15 (red), 30 (green), 45 (blue), 60 (yellow), and 75 (magenta) degrees as a function of fractional radius r/R, as inferred from the set of MPTS frequency-splitting coefficients obtained from the $\mathcal{R}$2010_66 observing run using modes with degrees up to $l = 1000$. Here, r is the radial distance from the center, and R denotes the radius of the Sun. The vertical dashed turquoise line marks the lower boundary of the convection zone. The error bars along each rotation profile represent $1\,\sigma$ formal uncertainties that were enlarged by a factor of 10. (Right) Same as left panel, except that from the table of the MPTS frequency-splitting coefficients only modes with degrees up to $l = 300$ were taken into account in the inversion procedure.

near the base of the convection zone ("tachocline") where the rotation rate shows a sharp transition from the differential rotation in the convection zone to a solid body like rotation in the radiative interior, and 3) the decrease of the rotation rate in the sub-surface layers with increasing radius at all latitudes depicted. The initial evidence of the SSL was presented by Rhodes et al. (1988) and by Korzennik et al. (1988). These results were confirmed quickly by Rhodes et al. (1990) and by Korzennik et al. (1990). In particular, the results presented by Rhodes et al. (1990) suggested that the angular velocity increased with increasing depth beneath the photosphere in the SSL at low-, medium, and high-latitudes, which is consistent with the results shown in both panels of Figure 30. Thus, Figure 30 confirms the lack of evidence for a reversal in the sign of the radial gradient at mid- and high-latitudes. The most obvious differences to note between these two panels are the steeper near-surface radial gradients in the rotation rate of the intermediate-degree inversion (right panel) for latitudes greater than or equal to 45 degrees, as can also been seen in the left panel of Figure 31.

It is generally believed that both shear layers play a crucial role for the solar dynamo (e.g., Charbonneau 2010). However, there is some controversy in the literature as to whether the near-surface shear changes sign at higher latitudes. Such change of sign in the range from 30° to 60° latitude has been found by, for example, Thompson et al. (1996), Kosovichev et al. (1997), and Corbard, & Thompson (2002). Barekat et al. (2014) found a change of sign as well, but at about 75° latitude. Moreover, Barekat et al. (2016) found the rotational shear at low latitudes (0° to 30°) to vary in-phase with the solar activity, varying by about ±10 percent over the period from 1996 to 2015. At high latitudes (60° to 80°), they found the rotational shear to vary in anti-phase with the solar activity. On the other hand, Rhodes et al. (1990), and Corbard et al. (2013) found no indication at all of a reversal in the sign of the radial gradient, in agreement with our results shown in Figure 30 and the left panel of Figure 31, respectively.

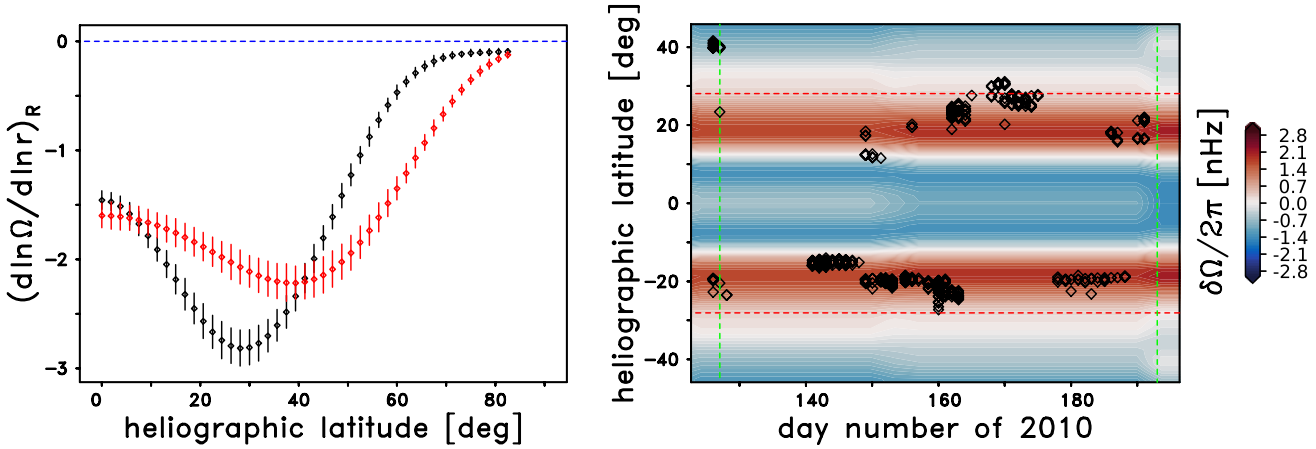

Figure 31. (Left) Logarithmic radial gradient of the rotation rate, $\mathrm{d}\ln\Omega/\mathrm{d}\ln r$, evaluated at the solar surface as a function of latitude. The high-degree inversion is shown in black, while the intermediate-degree inversion is shown in red. The error bars along each curve represent $1\,\sigma$ formal uncertainties that were enlarged by a factor of 200. The dashed horizontal blue line represents $\mathrm{d}\ln\Omega/\mathrm{d}\ln r = 0$. (Right) Heliographic latitude of individual sunspots as a function of the day of the year 2010, as inferred from HMI continuum intensity images. Color coded are superimposed the rotation-rate residuals, $\delta\Omega/2\pi$ measured in nHz, at a target depth of 0.99 fractional radii as a function of latitude and time, as inferred from RLS inversions of GONG, MDI, and HMI data. The mean to be subtracted was taken separately over the whole data set for GONG and for the combined MDI and HMI set. The horizontal dashed red lines delimit the range of heliographic latitudes between ± 28.1 degrees. The vertical dashed green lines mark the start and end of the 2010 MDI Dynamics Run on May 7th and July 11th, respectively.

In their comparative study of GONG and MDI data, Schou et al. (2002) concluded that the most significant differences in the rotational inversions arise not from the observations themselves but from the different frequency estimation analyses used by the two projects. Specifically, they found that the GONG pipeline results in substantially fewer fitted modes in certain regions of the l-ν plane. The most serious systematic differences in the results regarding the rotational inversions appear to be an anomaly in the MDI odd-order splitting coefficients around a frequency of 3.5 mHz and an underestimation of the low-degree rotational splittings in the GONG algorithm. The results from this comparative study may explain in some respects the different findings regarding the high-latitude reversal of the near-surface shear. However, it is to be noted that all previous studies of this shear did not include any high-degree splitting coefficients.

In order to quantify the differences in the shape of the radial gradient of the angular velocity that resulted from the two different rotational inversions that were shown in Figures 28 and 30, we computed the logarithmic radial gradient, $\mathrm{d}\ln\Omega/\mathrm{d}\ln r$, of the angular velocity at the solar surface as a function of heliographic latitude. The latitudinal dependence of the two different sets of radial gradients are shown in the left-hand panel of Figure 31, with the gradient that resulted from the high-degree inversion being shown in black and the gradient that resulted from intermediate-degree inversion being shown in red. It is apparent that these two curves are quite different in the magnitudes and locations of the peak gradients and in the widths of those peaks. The radial gradient that was derived from high-degree inversion peaks close to a value of -2.8, while the radial gradient from the intermediate-degree inversion peaks around -2.2. Furthermore, the gradient from the high-degree inversion peaks much closer to the solar equator and that peak is much narrower than the peak in

the gradient from the intermediate-degree inversion. In fact, the absolute value of $\mathrm{d}\ln\Omega/\mathrm{d}\ln r$ at the solar surface that came from the high-degree inversion peaks at a heliographic latitude of 28.1 degrees. This location is very similar to the latitude of the poleward side of the branch of the torsional oscillation that was approaching the solar equator during mid-2010. To see how closely the location of the steepest radial gradient of the angular velocity at the top of the SSL corresponded to the locations of the sunspots that were visible on the sun during the 2010 Dynamics Run, we employed a set of hourly HMI continuum intensity images that were obtained during that 66-day time interval. We then located all of these sunspots in the HMI images and we converted their pixel coordinates into the heliographic latitudes and Carrington longitudes. The latitudes of these spots are shown as a function of time in the right-hand panel of Figure 31. Out of the 407 sunspots, 384 of them had absolute values of their latitudes that were less than or equal to 28.1 degrees, or 94.35 percent. Only 23 of these spots were located at higher latitudes than the location of the peak radial gradient from the high-degree inversion, and most of those spots were located within a single active region at the beginning of the time interval.

The different colored bands that underlie the locations of the sunspots in the right-hand panel of Figure 31 are a set of rotational residuals computed by R. Howe (2019, private communication). These residuals were computed by the subtraction of a temporal mean from a two-dimensional rotational inversion of a combination of GONG, MDI, and HMI frequency-splitting coefficients. The two red bands show the latitudes where the angular velocity at a sub-photospheric depth of $0.01\,R_{\mathrm{sun}}$ was faster than the average angular velocity at that depth. Both of these bands represent the branch of the solar torsional oscillation that was moving toward the solar equator during mid-2010. Both of these red bands can clearly be seen to agree closely with the locations of the overwhelming majority of the sunspots that we identified in the HMI images. In addition, both of these bands appear to be bounded on their poleward sides by the two dashed red lines that denote the ± 28.1 degree latitudes where the absolute value of radial gradient of the surface angular velocity (i.e., the black curve in the left-hand panel of Figure 31) reached its peak value in our higher-degree rotational inversion. By contrast, the latitude of 39.4 degrees at which the radial gradient of the angular velocity went through its peak value in our lower-degree inversion (i.e., the red curve in the left-hand panel of Figure 31) shows no correlation with the locations of the majority of the sunspots.

8. CONCLUDING REMARKS AND OUTLOOK

Global helioseismology, that is the study of the Sun by means of its normal modes of oscillations, has revolutionized our knowledge of the Sun by revealing its large-scale structure and rate of rotation as functions of radial distance and latitude with unprecedented accuracy. However, what is still missing is an improved understanding of the near-surface layers of the Sun. These layers are believed to play a crucial role in the formation of the magnetic network, active regions, and sunspots, and thus are a key to the understanding of the mechanisms of solar activity and variability, at present possibly the most important unsolved problem in solar physics.

A straightforward approach to study the near-surface layers of the Sun is to employ precise frequencies of high-degree modes. Unfortunately, those modes do not appear as isolated, sharp peaks in the power spectra but rather as broad ridges of power. This is mainly for two reasons. First, any power spectrum computed for a specific target mode (l, m) contains contributions of power from modes with neighboring l and m because the spherical harmonic functions used in the spatial decomposition of the observed Dopplergrams are not orthogonal on that part of the Sun we observe. These so-called